### Title

Altered Redox Mitochondrial Biology in the Neurodegenerative Disorder Fragile X-Tremor/Ataxia Syndrome: Use of Antioxidants in Precision Medicine




### Journal

Molecular Medicine, 22(1)

### ISSN

1076-1551



### Authors

Song, Gyu
Napoli, Eleonora
Wong, Sarah
et al.



### Publication Date

2016

### DOI

10.2119/molmed.2016.00122

Peer reviewed

Cerebellum
DOI 10.1007/s12311-016-0779-8

ORIGINAL PAPER

# Altered Bioenergetics in Primary Dermal Fibroblasts from Adult Carriers of the *FMR1* Premutation Before the Onset of the Neurodegenerative Disease Fragile X-Associated Tremor/Ataxia Syndrome

**Eleonora Napoli**[1] · **Gyu Song**[1] · **Sarah Wong**[1] · **Randi Hagerman**[2,3] · **Cecilia Giulivi**[1,2]



**Abstract** Fragile X-associated tremor/ataxia syndrome (FXTAS) is a late onset neurodegenerative disorder, characterized by tremors, ataxia, impaired coordination, and cognitive decline. While all FXTAS individuals are carriers of a 55–200 CGG expansion at the 5′-UTR of the fragile X mental retardation gene (*FMR1*), also known as premutation, not all carriers develop FXTAS symptoms and some display other types of psychological/emotional disorders (e.g., autism, anxiety). The goal of this study was to investigate whether the mitochondrial dysfunction previously observed in fibroblasts from older premutation individuals (>60 years) was already present in younger (17–48 years), non-FXTAS-affected carriers and to identify the type and severity of the bioenergetic deficit. Since FXTAS affects mostly males, while females account for a small part of the FXTAS-affected population displaying less severe symptoms, only fibroblasts from males were evaluated in this study. Based on polarographic and enzymatic measurements, a generalized OXPHOS deficit was noted accompanied by increases in the matrix biomarker citrate synthase, oxidative stress (as increased mtDNA copy number and deletions), and mitochondrial network disruption/disorganization. Some of the outcomes (ATP-linked oxygen uptake, coupling, citrate synthase activity, and mitochondrial network organization) strongly correlated with the extent of the CGG expansion, with more severe deficits observed in cell lines carrying higher CGG number. Furthermore, mitochondrial outcomes can identify endophenotypes among carriers and are robust predictors of the premutation diagnosis before the onset of FXTAS, with the potential to be used as markers of prognosis and/or as readouts of pharmacological interventions.

**Keywords** Autism · Fragile X · Mitochondria · Neurodegeneration · Premutation · Triplet nucleotide diseases · Endophenotyes · Mitochondrial network

## Introduction

Fragile X-associated tremor/ataxia syndrome (FXTAS) is caused by a modestly expanded CGG nucleotide repeat (55–200) in the 5′-untranslated region (5′-UTR) of the fragile X mental retardation gene *FMR1*. This expansion is known as the "premutation," in contrast to the "full mutation" which entails a larger expansion (>200 CGG) in the same gene. The full mutation is causative of the fragile X syndrome (FXS), the most common inherited form of mental retardation. The *FMR1* messenger RNA (mRNA) is rapidly translated at synapses in an activity-dependent manner [1], where it constrains local synaptic protein translation [2]. FMRP, the protein product of *FMR1*, critically regulates synaptic function, and its transcriptional loss leads to FXS [3], syndrome

**Electronic supplementary material** The online version of this article (doi:10.1007/s12311-016-0779-8) contains supplementary material, which is available to authorized users.

✉ Cecilia Giulivi
cgiulivi@ucdavis.edu

[1] Department of Molecular Biosciences, School of Veterinary Medicine, University of California Davis, 1089 Veterinary Medicine Dr., VetMed 3B, Davis, CA 95616, USA

[2] Medical Investigation of Neurodevelopmental Disorders Institute (M. I. N. D.), University of California Davis, Sacramento, CA 95817, USA

[3] Department of Pediatrics, University of California Medical Center, Sacramento, CA 95817, USA

Published online: 18 April 2016

associated with a high co-morbidity with autism [4, 5]. By contrast, carriers of the premutation show normal or elevated *FMR1* mRNA expression and, when affected with FXTAS, neurodegeneration with neuronal intranuclear inclusions that contain the CGG repeat mRNA and various proteins [5, 6].

Research to date has focused on how the CGG repeat might trigger neurodegeneration through a gain-of-function RNA mechanism [7], but critical aspects of disease pathology cannot be explained by a purely RNA-mediated process. Neuronal intranuclear inclusions in FXTAS brains resemble more those observed in Huntington's disease, another triplet nucleotide disease, and other protein-mediated neurodegenerative disorders rather than those observed in RNA-mediated disorders. Consistent with this view, fibroblasts from older premutation carriers (>60 years old) show mitochondrial pathology similar to that present in Huntington's disease [8, 9]. Cells from carriers without FXTAS (named hereafter as asymptomatic) exhibited mitochondrial dysfunction characterized by lower Complex IV (34 % of controls) and Complex V (71 % of controls) activities [8]. While these changes were also observed in those carriers affected with FXTAS, more marked deficits in Complex V (38 % of controls), with additional decreases in Complex I (75 % of controls; [8]), were observed in these individuals. Thus, the characteristics of the mitochondrial dysfunction and the ubiquitin-positive neuronal inclusions seem to account for a pathologic hallmark of protein-mediated rather than RNA-mediated neurodegeneration [2].

Recently, the paradox of the RNA-mediated vs. protein-mediated toxicity in FXTAS, although still controversial [10], has been partly explained by demonstrating that CGG repeats trigger repeat-associated non-AUG-initiated (RAN) translation [2] of a cryptic polyG-containing protein, FMR1polyG. This FMR1polyG accumulated in ubiquitin-positive inclusions in *Drosophila* and mammalian cell cultures carrying the expansion, and in FXTAS patient brains [2]. Hence, the molecular pattern observed in FXTAS could be analogous to that in Huntington's disease, in which at least nine potential toxic species can be foreseen, including the "traditional" polyQ-mutated huntingtin protein [11].

While mitochondrial dysfunction was present in fibroblasts from older carriers of the premutation and more enhanced in those with FXTAS [8], a critical question is whether mitochondrial dysfunction is evident in adult carriers at a relatively younger age without overt clinical symptoms. Considering that FXTAS affects mostly males, while females account for only a small part of the FXTAS-affected population displaying less severe symptoms, only males were evaluated in this study. Here, we evaluated (i) whether mitochondrial dysfunction was present in fibroblasts from younger adults with the premutation who did not meet clinical criteria for FXTAS and (ii) the nature and severity of the putative dysfunction. The relevance of this study was to establish whether mitochondrial outcomes could serve as early markers of prognosis of the disease or as readouts of the efficacy of therapies before the occurrence of FXTAS symptoms. Although it could be argued that primary dermal fibroblasts do not constitute an appropriate model to address mitochondrial dysfunction (or any other outcome) in a syndrome with clear CNS symptoms, fibroblasts from premutation patients do present overexpression of *FMR1* transcript with levels comparable to those observed in neurons, and biochemical changes in fibroblasts [12] followed those exhibited by lymphocytes (Napoli et al., in revision), neurons [13, 14], and brain from carriers [12] and murine models of the premutation [14]. In addition, fibroblasts obtained from skin biopsies have the advantage of being relatively less invasive than muscle biopsy—which is usually used for diagnosing mitochondrial diseases—and avoids the issue of using postmortem tissues (with the problem of the postmortem interval and cause of death) for brain samples.

## Materials and Methods

### Characteristics of the Subjects Enrolled in This Study

The study group named "control" consisted of 12 individuals, all male, with a mean age of 29 ± 3 years (mean ± SEM) with CGG repeats at the 5′-UTR of *FMR1* of 30 ± 1 (Table 1). The group named "premutation" was constituted by five premutation carriers, all men, with an age of 29 ± 5 years and CGG repeats of 106 ± 19 (Table 1). No significant difference in terms of age (Student's *t* test, $p = 0.496$) was observed between these groups, whereas a highly significant difference was observed in terms of CGG length (Student's *t* test, $p = 0.008$).

### Cell Culture Conditions

Fibroblasts were grown to 75 to 80 % confluence to evaluate mitochondrial outcomes. The passage number of cells used for all the measurements was between 8 and 12. Cells were grown in a 1:1 solution of AmnioMAX-C100 and RPMI-1640 Basal Medium supplemented with 10 % fetal bovine serum (Invitrogen), 1× penicillin/streptomycin/glutamine (Invitrogen), 1 % non-essential amino acids (Invitrogen), and 1:250 Fungizone (J R Scientific, Woodland, CA, USA) as previously described elsewhere.

### Mitochondrial Outcomes

Mitochondria from fibroblasts were evaluated by polarography under phosphorylating conditions (adenosine triphosphate (ATP) producing) with NAD- and FAD-linked substrates [8]. Briefly, oxygen consumption in digitonin-permeabilized cells was evaluated using a Clark-type oxygen

**Table 1** Demographic and clinical characteristics of the study participants and outcomes measured in primary dermal fibroblasts obtained from each individual

| Clinical group | Age (years) | CGG number | Outcomes measured |
|---|---|---|---|
| Control 1 | 18 | 23 | Pol; NQR, CCO, ATPase, CS, CN, Del, Conf |
| Control 2 | 21 | 25 | Pol; NQR, CCO, ATPase, CS, CN, Del. |
| Control 3 | 29 | 29 | Pol; NQR, CCO, ATPase, CS, CN, Del |
| Control 4 | 36 | 30 | Pol; NQR, CCO, ATPase, CS, CN, Del; Conf. |
| Control 5 | 20 | 29 | Pol; NQR, CCO, ATPase, CS, CN, Del |
| Control 6 | 41 | 43 | Pol; NQR, CCO, ATPase, CS, CN, Del |
| Control 7 | 12 | 34 | Pol; NQR, CCO, ATPase, CS, CN, Del |
| Control 8 | 26 | 34 | Pol; CS, CN, Del |
| Control 9 | 24 | 30 | Pol; CS, CN, Del |
| Control 10 | 29 | 30 | Pol; CS, CN, Del |
| Control 11 | 25 | 29 | Pol; CS, CN, Del |
| Control 12 | 16 | 30 | Pol; CS, CN, Del |
| Control 13 | 46 | 30 | NQR, CCO, ATPase, CS, CN, Del |
| Control 14 | 39 | 30 | Pol; NQR, CCO, ATPase, CS, CN, Del |
| Control 15 | 40 | 30 | Pol; NQR, CCO, ATPase, CS, CN, Del, Conf |
| Control 16 | 34 | 30 | Pol; NQR, CCO, ATPase, CS, CN, Del, Conf |
| Premutation 1 | 17 | 170 | Pol; NQR, CCO, ATPase, CS, CN, Del, Conf. |
| Premutation 2 | 23 | 77 | Pol; NQR, CCO, ATPase, CS, CN, Del, Conf. |
| Premutation 3 | 33 | 82 | Pol; NQR, CCO, ATPase, CS, CN, Del |
| Premutation 4 | 48 | 127 | Pol; NQR, CCO, ATPase, CS, CN, Del, Conf |
| Premutation 5 | 25 | 72 | Pol; CS, CN, Del |

*Pol* activities evaluated by polarography, namely, NADH oxidase, succinate oxidase, and α-glycerophosphate oxidoreductase activities, *CCO* cytochrome *c* oxidase activity measured spectrophotometrically, *CS* citrate synthase activity, *NQR* NADH decylubiquinone oxidoreductase activity, *CN* mtDNA copy number, *Del* mtDNA deletions in segments encoding for *ND4* and *CYTB*, *Conf* mitochondrial morphology/distribution by confocal microscopy

electrode (Hansatech, King's Lynn, UK) as described [15]. Two million cells were added to the oxygen chamber in a buffer containing 0.22 M sucrose, 50 mM KCl, 1 mM EDTA, 10 mM $KH_2PO_4$, and 10 mM HEPES, pH 7.4. Oxygen consumption rates were evaluated in the presence of (i) 1 mM ADP plus 1 mM malate-10 mM glutamate followed by the addition of 5 μM rotenone; (ii) 10 mM succinate followed by the addition of 10 mM malonate; and (iii) 10 mM α-glycerophosphate followed by the addition of 3.6 μM antimycin A. The activities of mitochondrial NADH oxidase, succinate oxidase, and α-glycerophosphate were evaluated as the difference of oxygen uptake recorded before and after the addition of rotenone, malonate, and antimycin A, respectively. Specific activities of Complex I, IV, and V were measured spectrophotometrically as described before [9, 16, 17], assessing respectively the activities of the rotenone-sensitive NADH decylubiquinone oxidoreductase, KCN-sensitive cytochrome *c* oxidase, and oligomycin-sensitive ATPase.

The following mitochondria-dependent outcomes were assessed in intact cells in phenol red-free RPMI-1640 media (Life Technologies, Grand Island, NY, USA), supplemented with 10 mM glucose and 2 mM glutamine: (i) ATP-linked oxygen uptake (or State 3-dependent oxygen uptake rate) calculated as the difference between basal and oligomycin-induced State 4 oxygen uptake rates; (ii) State 4, residual respiration after inhibition of ATP synthesis with the ATPase-specific inhibitor oligomycin (2 μM final concentration); (iii) maximal respiratory capacity, or State 3u, oxygen uptake rate in the presence of the uncoupler carbonyl cyanide-4-(trifluoromethoxy) phenylhydrazone (FCCP) (0.2 μM final concentration); (iv) respiratory control ratio, obtained by the ratio between oligomycin-sensitive and oligomycin-resistant oxygen uptake; (v) respiratory control ratio under uncoupling conditions (RCRu), calculated as the ratio between State 3u and State 4; and (vi) spare respiratory capacity, calculated as State 3u-dependent oxygen uptake normalized by the basal respiration. Citrate synthase activity (a biomarker for mitochondrial matrix) was evaluated by enzymatic analysis as previously described [8].

### Mitochondrial DNA Copy Number and Deletions

For the evaluation of mitochondrial DNA (mtDNA) copy number and deletions in fibroblasts, genomic DNA was isolated from $1 \times 10^6$ cells from fibroblasts using the Gentra

Puregene Cell and Tissue Kit (Qiagen, Valencia, CA, USA) and following the manufacturer's recommendations for cell samples. Concentration and purity of DNA were measured at 260 and 280 nm on a Tecan Infinite M200 NanoQuant (Tecan, Austria). DNA was diluted to 0.63 ng/μl and served as stock DNA template for qPCR. Following DNA extraction, changes in mtDNA copy number and deletions were evaluated by using dual-labeled probes as described in details elsewhere [15, 18]. Relative mtDNA copy number per cell was assessed by a comparative Ct method, using the following equation: $\text{mtDNA/nDNA} = 2^{-\Delta Ct}$, where $\Delta Ct = Ct_{\text{mitochondrial}} - Ct_{\text{nuclear}}$. Each sample was analyzed in triplicates. The *ND1* gene copy number was normalized by the single copy nuclear gene (pyruvate kinase) to reflect the mtDNA copy number per cell whereas the ratios of *CYTB* or *ND4* copy number normalized to that of *ND1* reflected mtDNA deletions in the major arc.

### Mitochondria Morphology and Network Analyses

Morphological analysis of mitochondria was performed on fibroblasts from four control and four premutation stained with MitoTracker Red as previously described [9, 16]. Cells ($1 \times 10^5$) were seeded on sterile coverslips, grown overnight at 37 °C, and then stained with 0.5 μM MitoTracker Red CMXRos (Molecular Probes Inc., Eugene, OR, USA) diluted in growth media for 30 min at 37 °C. After staining, cells were washed with media and fixed in 3.7 % formaldehyde for 10 min. Fixed cells were washed again in PBS, blocked/permeabilized for 30 min in blocking buffer at 20–22 °C, counterstained with 1 μg/ml DAPI, and mounted on glass slides with antifading mounting media (Dako). At least 10 fields per cell line were imaged using an Olympus FV1000 laser scanning confocal microscope (excitation and emission wavelengths 594 and 660 nm, respectively) with ×60 magnification and zoom values between 3 and 4. Images were analyzed with the ImageJ software discarding the color information and adjusting the threshold to minimize the background level. Pattern of mitochondrial network was analyzed using the Fiji (ImageJ) plugin MitoMap, and the percentage of cells exhibiting disrupted mitochondrial network were calculated as described in [19].

### Statistics

Statistical analysis was performed with the Student's *t* test for comparisons between control and premutation groups, unless otherwise noted. Statistical significance level was set at a *p* value ≤0.05. Post hoc analysis was used to compute the achieved power (given an alpha of 0.05, sample size of 12 for control and 5 for premutation groups), which resulted to be (one-tail) 1.00 for NADH oxidase, succinate oxidase, and alpha-glycerophosphate oxidase activities; 0.96 for citrate synthase activity; 1.00 for NADH-decylubiquinone oxidoreductase (NQR), CCO, and ATPase activities; 0.320 for mtDNA copy number; 0.86 and 1.00 respectively for *CYTB* and *ND4* deletions; 0.96 for oxygen uptake under State 3 and 1.00 for oxygen uptake under State 4 and State 3u; and 1.00 for mitochondrial network fragmentation (G*Power software, version 3.0.10).

## Results and Discussion

### Deficits in Bioenergetics and Higher Citrate Synthase Activity in Fibroblasts from Premutation Carriers

Primary, dermal fibroblasts were obtained from 12 controls (mean ± SEM, age in years and CGG repeats: 29 ± 3 and 30 ± 1; Table 1) and 5 premutation carriers (29 ± 5 and 106 ± 19; Table 1). To preserve the intracellular environment of which mitochondria are a part, we proceeded to use the selective permeabilization of the plasma membrane of fibroblasts with digitonin to give mitochondrial substrates access to mitochondria and be able to evaluate the rate of oxygen uptake under phosphorylating conditions (i.e., in the presence of ADP to generate ATP). Measurement of mitochondrial oxygen consumption rates is a convenient technique to assess mitochondrial functional integrity. Additionally, the ability of uncouplers and/or various metabolic inhibitors to alter the rate of oxygen consumption in a specified and regulated manner is a further indicator of the functional integrity of mitochondria.

For this study, different segments of the electron transport system were tested for their capacity to generate ATP in fibroblasts from control and premutation individuals: NADH oxidase, using NAD-linked substrates and comprising Complexes I, III, IV, and V; succinate oxidase, using FAD-linked substrates and comprising Complexes II, III, IV, and V; and α-glycerophosphate oxidoreductase, encompassing Complexes III, IV, and V. NADH oxidase, succinate oxidase, and α-glycerophosphate oxidoreductase in cells from carriers were respectively 70 % ($p = 0.009$), 55 % ($p = 0.013$), and 70 % ($p = 0.044$) of control values (Fig. 1a, Supplementary Table 1). These results suggested a generalized oxidative phosphorylation deficit more pronounced at the level of succinate oxidase compared to NADH oxidase (20 % lower) suggesting a lower capacity to oxidize FAD-linked substrates (such as fatty acids) vs. carbohydrates (as NAD-linked substrates). When activities were normalized by citrate synthase, a biomarker of mitochondrial matrix (Fig. 1b), differences observed in premutation vs. controls were magnified to 59 % ($p = 0.031$), 42 % ($p = 0.0006$), and 64 % ($p = 0.060$) of controls, respectively, for NADH oxidase, succinate oxidase, and α-glycerophosphate oxidoreductase. The more marked differences in the ATP-linked oxygen uptake supported by various substrates between diagnostic groups when normalized to citrate synthase were ascribed to the significantly

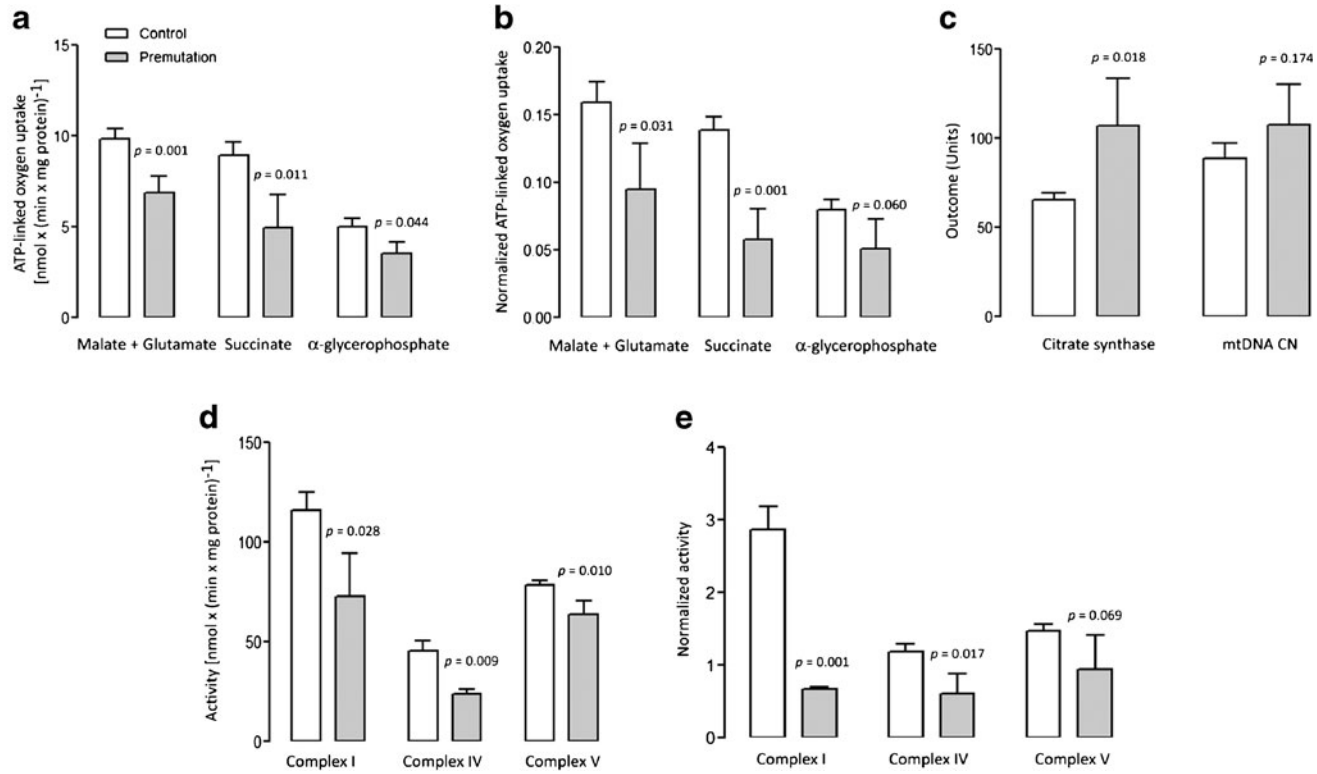


**Fig. 1** Mitochondrial outcomes in control and premutation fibroblasts. OXPHOS measurements were carried out in fibroblasts from a panel of 12 controls (*white*) and 5 premutation carriers (*gray*), expressed as nmol $O_2 \times (\text{min} \times \text{mg protein})^{-1}$ and shown not normalized (**a**) or normalized (**b**) by citrate synthase activity (**c**). Mitochondrial DNA copy number per cell (**c**) is the gene copy ratio of the mitochondrial gene *ND1* to the single-copy nuclear gene *pyruvate kinase*. Values for mtDNA copy number were divided by 10 to fit the same scale. Activities of Complex I (NQR), Complex IV (or cytochrome *c* oxidase), and Complex V (or $F_oF_1$-ATPase) were expressed as nmol × (min × mg protein)$^{-1}$ and shown not normalized (**d**) or normalized (**e**) by citrate synthase activity. Data were shown as mean ± SEM for each group. Statistical analysis was performed with the Student's *t* test between control and premutation. Individual values for premutation fibroblasts, compared to the 95 % CI, are reported in Supplementary Table 1

higher activity of this matrix biomarker in premutation individuals relative to controls (1.6-fold higher; $p = 0.009$; Fig. 1c, Supplementary Table 1).

Increased citrate synthase activity might indicate an effort to increase mitochondrial mass as a result of mitochondrial proliferation via the activation of feedback loops to compensate for a compromised electron transport among Complexes. To evaluate mitochondrial mass, we assessed the mtDNA copy number per cell. However, the lower OXPHOS capacity supports the concept that cells carrying the premutation underwent a remodeling of mitochondria with a relative decrease in the inner membrane components (where the Complexes of the electron transport system are allocated, i.e., Complex I, II, III, IV, and V) to the matrix ones (citrate synthase). This could be explained by an abnormal matrix-to-cristae surface area or volume ratio, due to changes in cristae configuration/restructuring [20].

To discern specific, intrinsic defects in the Complexes vs. altered transfer of electrons among Complexes (as observed by polarography), specific activity of Complexes I, IV, and V were assessed (Fig. 1d, Supplementary Table 1) in fibroblasts from controls and premutation carriers. As reported above for NADH oxidase and cytochrome *c* oxidase activities, lower specific activity of Complex I (63 % of controls, as judged by the NQR) and Complex IV (52 % of controls) was noted in premutation cells (Fig. 1d; $p = 0.028$ and $p = 0.009$, respectively). Upon normalization by citrate synthase, Complex I and Complex IV activities in cells from carriers of the premutation were 23 and 51 % of controls ($p = 0.0009$ and $p = 0.017$, respectively, Fig. 1e). A decrease in the oligomycin-sensitive ATPase activity was observed in premutation cells, before (81 % of controls; $p = 0.010$) and after (64 % of controls; $p = 0.069$) normalization by citrate synthase (Fig. 1d, e). As observed in other mitochondrial diseases, the path of electron flow between Complexes (as tested by polarography) did not seem to be as affected as the specific activities of these Complexes. This observation—that the oxygen uptake is less impaired than the marked reduction in the activity of the various Complexes—has been termed "the oxidative reserve" [21, 22]. This reserve implies that the reduction in the supply of reducing equivalents by the individual Complexes is not affecting as much the rate of oxygen uptake since the activity of the Complexes tested is greater than the rate of oxygen uptake. This association will hold until a critical value is

reached, beyond which a reduction of oxygen uptake is observed. Clearly, this association will also be modified or influenced by the workload (or oxygen demand). This might explain why in some carriers a significant reduction in ATP-linked oxygen uptake does not result in a phenotype while in others the decreased flow of reducing equivalents leads to a reduction of ATP provision and the occurrence of a phenotype or symptoms.

### Lower ATP-Linked Oxygen Uptake in Mitochondria from Intact Fibroblasts from Premutation Carriers

ATP-linked oxygen uptake in intact cells supplemented with glucose and glutamine, inferred by the oligomycin-sensitive oxygen uptake, was 3.3-fold higher ($p = 0.006$) in fibroblasts from control than premutation (Fig. 2a, Supplementary Table 1). Addition of FCCP, to uncouple respiration in order to obtain the maximum oxygen uptake rate, increased the rate of oxygen uptake above State-3 rate for both controls (2.7-fold) and carriers of the premutation (6.3-fold; Fig. 2a, Supplementary Table 1). Therefore, the oxygen consumption was limited in both (and more so in carriers) by the capacity of the ATPase. Consistent with these results, the normalized ATPase activity was 36 % lower than in carriers (Fig. 1d).

Coupling between ATP synthesis and electron flow was evaluated by using the respiratory control ratio (RCR), calculated as the ratio between oligomycin-sensitive and oligomycin-resistant oxygen uptake. The RCR was lower in cells from carriers than controls (28 % of controls; $p = 0.013$; Fig. 2b, Supplementary Table 1) indicating that the electrochemical potential generated by the electron flow among Complexes was not harnessed efficiently as ATP. The RCR was also evaluated under conditions of maximum oxygen uptake (uncoupling conditions, RCRu) over that of oligomycin-induced State 4 in intact fibroblasts. Mitochondria from premutation cells showed 48 % of the RCRu values observed in controls ($p = 0.011$; Fig. 2b, Supplementary Table 1). "True" increased uncoupling is the result of increases in State 4 oxygen uptake [23–25] due to higher proton leak-mediated oxygen uptake (e.g., loss of inner membrane intactness or increased permeability) and/or electron leak as reactive oxygen species production [26]. In the case of premutation carriers, the lower RCR and RCRu seemed to result from a combination of a lower rate of electron flow across the Complexes (State 3 and State 3u were 30 and 70 % of controls; Fig. 2a) and higher State 4-linked oxygen uptake (1.7-fold of controls; Fig. 2a) rather than by a net increase in State 4-linked oxygen uptake.

The spare respiratory capacity, defined as the difference between ATP produced by oxidative phosphorylation at basal and at maximal respiratory activity, although not statistically significant, was in average 1.6-fold higher in controls than premutation ($p = 0.179$; Fig. 2b, Supplementary Table 1). Considering that the spare respiratory capacity is critical for neuronal susceptibility to cellular stress [27], this result suggests a trend towards lower capacity to adapt to increasing energy demands in the premutation. Resting neurons utilize about 6 % of their maximal respiratory capacity, while active neurons up to 80 % [28], then even small decreases in reserve respiratory capacity may enhance neuronal vulnerability, predisposing the tissue to energy deficits and neurodegeneration.

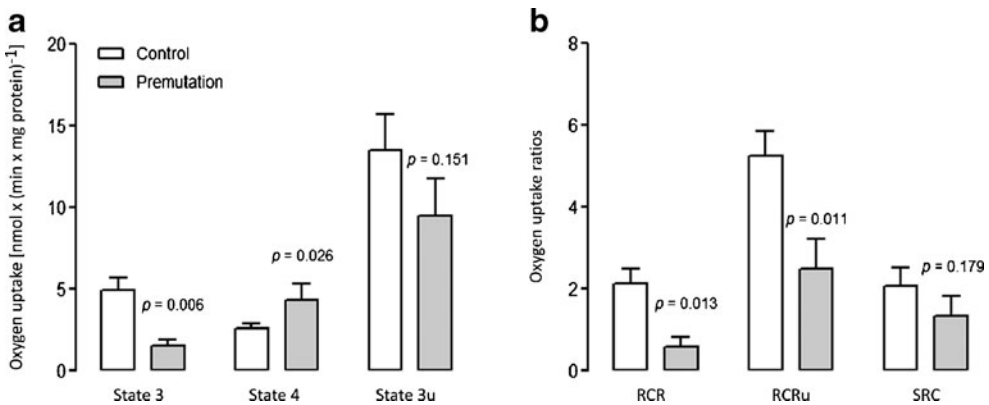


**Fig. 2** Respiratory capacity and coupling in fibroblasts from controls and premutation. **a** Oxygen uptake rates in intact cells in the presence of 10 mM glucose in RPMI, 2 mM glutamine, and no phenol red, as described in the "Materials and Methods" section. Rates were recorded before and after the addition of 2 μM oligomycin and subsequent uncoupling with 0.2 μM FCCP. State 3 (difference between total oxygen uptake and oligomycin-resistant oxygen uptake) represents the ATP-linked oxygen uptake; State 4 (or oligomycin-resistant oxygen uptake) is an index of proton leak/ROS production; State 3u (oxygen uptake in the presence of the uncoupler FCCP) is the maximal oxygen uptake capacity. **b** RCR (respiratory control ratio) was calculated as the ratio between oligomycin-sensitive and oligomycin-resistant oxygen uptake rates. Respiratory control ratio under uncoupling conditions (RCRu) was (State 3u) × (State 4)$^{-1}$. SCR (spare respiratory capacity) was calculated as State 3u-dependent oxygen uptake normalized by the basal respiration. Control (*white*, $n = 12$) and premutation carriers (*gray*, $n = 5$). Statistical analysis was performed with the Student's *t* test for comparisons between control and premutation. Individual values for premutation fibroblasts, compared to the 95 % CI, are reported in Supplementary Table 1

### Abnormal Mitochondrial Morphology and Disrupted Network in Fibroblasts from Premutation Carriers

Mitochondrial function is tightly associated with dynamics, in which fusion-fission and clearance of mitochondria control not only the shape but also bioenergetics, allowing mitochondria to interact with each other; without such dynamics, the mitochondrial population consists of autonomous organelles that have impaired function [29]. To this end, mitochondria morphology, activity, and distribution were tested in fibroblast mitochondria from four premutation carriers and four controls by using confocal microscopy (subjects indicated in Table 1, Fig. 3, and Supplementary Fig. 1). Mitochondria were visualized by using MitoTracker Red, dye which is accumulated in mitochondria in favor of a membrane potential [30]. No differences were recorded in the intensity of the MitoTracker staining (normalized by cell area) in the two groups (mean $\pm$SD = 31 $\pm$ 2 and 26 $\pm$ 4 respectively, $p = 0.275$) suggesting that the degree of uncoupling between electron transport and ATP production recorded in the premutation fibroblasts as RCR was not enough to produce perturbations in the mitochondrial membrane potential able to affect the mitochondrial accumulation of the MitoTracker dye.

In terms of morphology, mitochondria in control cells looked elongated and tubular and as part of an organized network, whereas in premutation carriers they appeared more fragmented (1.7-fold, $p = 0.026$) with increased perinuclear localization and a more disorganized and "random" distribution (Fig. 3a and Supplementary Fig. 1). A strong direct correlation was noted between CGG repeat number and degree of the mitochondrial network fragmentation (Fig. 3b). These results suggested either an increased fission not met by the clearance of fragmented mitochondria (mitophagy) and/or issues related to the cellular transport of mitochondria, issues that seemed to increase in severity with the increase in CGG repeats.

### Extent of the CGG Expansion Correlates Inversely with ATP-Linked Oxygen Uptake and Coupling, and Directly with Citrate Synthase Activity

It has been shown that increasing CGG repeat size correlates strongly with the severity of FXTAS symptoms in older individuals [31] as well as with the degree of mitochondrial dysfunction [8, 12]. In support of this concept, a strong correlation between CGG repeats and fragmented mitochondrial network was noted in fibroblasts from younger premutation individuals (Fig. 3). Similarly, a strong inverse correlation was obtained between CGG repeat size and ATP-linked oxygen uptake (NADH- and succinate-oxidase activities, State 3), ATPase activity, and uncoupling, while a significant positive correlation was present between CGG repeat expansion and citrate synthase activity (Table 2). An almost significant correlation was obtained between CGG repeat expansion and RCRu, and alpha-glycerophosphate oxidoreductase activity, $p < 0.1$; Table 2).

### Mitochondrial Outcomes as Predictors of the Premutation Diagnosis

In order to evaluate whether mitochondrial outcomes could be used as reliable predictors of the premutation diagnosis, a hierarchical clustering (also called agglomerative hierarchical clustering or AHC) was performed. AHC starts with each point (row) as its own cluster. At each step, the clustering process calculates the distance between each cluster and combines the two clusters that are closest together. This combining continues until all the points are in one final cluster. Based on the cutoffs set by our analysis, the clustering tree gets cut at a certain point. The combining record is portrayed as a tree, called a dendrogram, with the single points as leaves, the final single cluster of all points as the trunk, and the intermediate cluster combinations as branches. The analysis was first conducted using exclusively those mitochondrial outcomes for which data was available for all the cell lines (namely, NADH oxidase, succinate oxidase, $\alpha$-glycerophosphate oxidoreductase, cytochrome *c* oxidase, and citrate synthase activities, as well as mtDNA copy number and deletions; Fig. 4a). Subsequently, the same analysis was performed including the data on individual CGG expansions (Fig. 4b).

The AHC analysis done with mitochondrial outcomes only classified the donors into three major clusters, namely, cluster 1 ($n = 9$; all controls except premutation no. 5), cluster 2 ($n = 3$, all controls), and cluster 3 ($n = 5$, all premutation carriers except control no. 4; Fig. 4a). The inclusion of the CGG size slightly modified the composition of the clusters, with clusters 1 and 2 represented by an $n = 7$ each (all controls except premutation no. 2 and no. 5 for clusters 1 and 2, respectively), and cluster 3, including the three premutation individuals with the most affected mitochondrial outcomes and longest CGG expansion. Thus, the inclusion of the hallmark of this genetic disease (the CGG repeats) did not influence significantly the clustering of subjects and both analyses identified cluster 3 as the one with the most severe mitochondrial dysfunction. Considering the absence of mitochondrial dysfunction in premutation no. 5, the algorithm clustered this sample with the rest of the controls in both analyses. Conversely, with the first AHC, one of the controls (control no. 4) was included in cluster 3 among premutation samples, likely due to its low cytochrome *c* oxidase activity and presence of mtDNA deletions.

To test which analysis was a better predictor of the occurrence of the premutation diagnosis, a diagnostic test evaluation was performed (Fig. 4c). Both analyses were suitable indicators of the premutation diagnosis, with the analysis performed with mitochondrial outcomes only having a higher

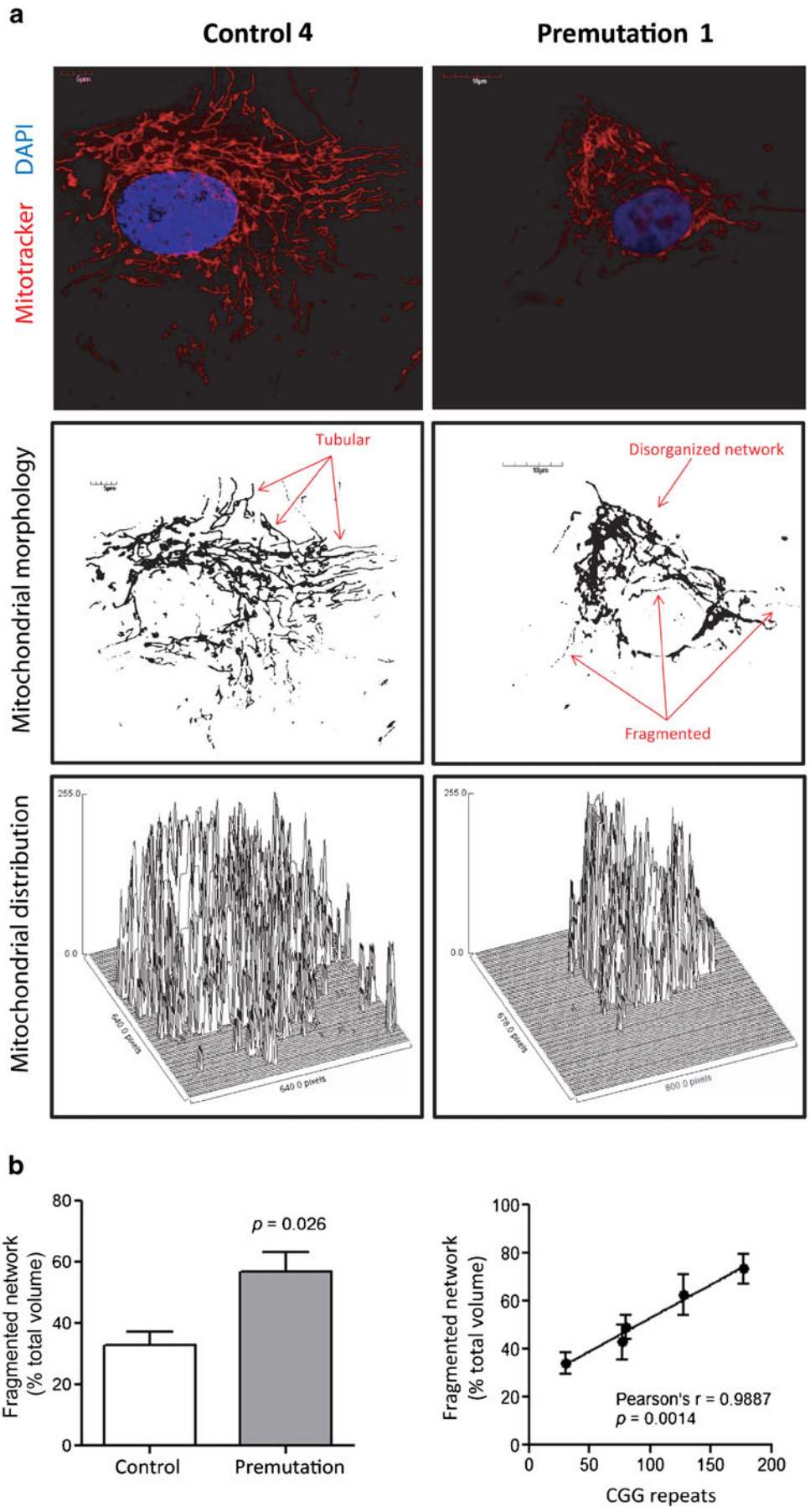
a
Control 4
Premutation 1
Mitotracker DAPI
Mitochondrial morphology
Tubular
Disorganized network
Fragmented
Mitochondrial distribution
255.0
0.0
640.0 pixels
640.0 pixels
255.0
0.0
678.0 pixels
800.0 pixels
b
Fragmented network (% total volume)
p = 0.026
Control
Premutation
Fragmented network (% total volume)
Pearson's r = 0.9887
p = 0.0014
CGG repeats

◀ **Fig. 3** Morphological analysis and mitochondrial distribution in fibroblasts from controls, premutation, and FXTAS. Slides for confocal analysis were prepared and stained as described in the "Materials and Methods" section. Image acquisition was performed with an Olympus FV1000 laser scanning confocal microscope with ×60 magnification and zoom values between 3 and 4. Images show fibroblasts obtained by control (control no. 4 in Table 1) and a premutation (premutation no. 2 in Table 1). Representative images of all control and premutation cell lines used for the morphological analysis are shown in Supplementary Figure 1. **a** *Top panels* show mitochondria stained with MitoTracker Red CMXRos (*red*) and nuclei stained with DAPI (*blue*). *Mid panels* show mitochondria morphology and distribution. Image was obtained with the ImageJ software discarding the color information and adjusting the threshold to minimize the background level. Images show a more disorganized mitochondrial network in cells from premutation individuals, with an increased fragmented/circular mitochondria and decreased tubular network in FXTAS cells. *Bottom panels* show surface plots obtained with the ImageJ software and display the perinuclear mitochondrial distribution observed in cells from premutation and FXTAS, compared to a more uniform cellular distribution in controls. **b** A statistically significant difference was observed in the percentage of disrupted/fragmented mitochondrial network in fibroblasts from premutation ($n=4$) relative to control ($n=4$). Statistical analysis was performed by using Student's $t$ test. The presence of a strong direct correlation between CGG repeat number and degree of the mitochondrial network disruption was also noted. At least 10 cells per line were imaged and analyzed with the Fiji's MitoMap plugin. Relative volumes ($V_s$) were calculated as described in [19]. Objects with $V_s \leq 20$ % of total cellular $V_s$ were considered fragmented

sensitivity, or probability that a test result will be positive when the condition is present. Conversely, the inclusion of the CGG size increased by 11 % the test's specificity (probability that a test result will be negative when the disease is not present).

## Characterization of Endophenotypes Among Premutation Carriers

The onset and/or progression of the disease could be different among carriers. In support of this concept, the AHC analysis based on mitochondrial outcomes (Fig. 4a) showed all fibroblasts from premutation carriers clustered together, except for premutation no. 5, the only premutation cell line showing oxidative phosphorylation capacity comparable to or higher than controls (Fig. 4a and Supplementary Table 1). The four premutation carriers included in cluster 3 presented combined deficits at the level of Complex I, II, IV, and/or V (Supplementary Table 1), with the most consistent and significant deficiency found at the levels of Complexes I, II, and IV, accompanied by deficits in Complexes III and V in premutation nos. 1, 3, and 4 (Supplementary Table 1). Citrate synthase activity, a mitochondrial matrix biomarker, was higher than the 95 % CI in four carriers, with the exception of premutation no. 2 (excluded by cluster 3 when the AHC analysis was performed with mitochondrial outcomes and CGG repeat length, Fig. 4b), with a lower activity than the 95 % CI (Supplementary Table 1).

In terms of ATP production, respiratory capacity, and coupling, all carriers included in cluster 3 showed lower ATP-linked oxygen uptake (State 3), accompanied by a lower RCR (Supplementary Table 1). Three of the five premutation individuals (all belonging to cluster 3) had increased State 4 rates (Supplementary Table 1), index of "true" mitochondrial uncoupling, and lower spare respiratory capacity (SRC).

Given that mitochondrial activities ≤30 % for cells in culture are considered as the threshold for minor diagnostic criteria of mitochondrial respiratory system disorders (whereas ≤20 % is a major; [32]), premutation carriers no. 2, no. 3, and no. 4 have 3 of 12 outcomes fulfilling the ≤30 % threshold. However, this well-established approach relies on significant decreases in mitochondrial electron transport Complex activities and/or the occurrence of known pathogenic mitochondrial DNA mutations [32]. When less stringent criteria are used (i.e., comparison with the 95 % CI), 80 % of the carriers exhibited values representative of mitochondrial dysfunction in at least 10 of the 14 mitochondrial outcomes measured.

As indicated above, no statistically significant differences in the mean mtDNA copy number per cell or deletions in the

**Table 2** Correlation parameters between CGG repeats and mitochondrial outcomes in fibroblasts from control and premutation

| Outcome | Pearson's $r$ | $p$ value |
|---|---|---|
| ATP-linked oxygen uptake (substrate) | | |
| Malate-glutamate | −0.487 | **0.040** |
| Succinate | −0.468 | **0.050** |
| α-Glycerophosphate | −0.407 | 0.094 |
| Complex activities | | |
| Complex I | −0.119 | 0.849 |
| Complex IV | −0.222 | 0.720 |
| Complex V | −0.581 | 0.304 |
| ATP-linked oxygen uptake and related parameters in intact cells | | |
| State 3 | −0.575 | **0.025** |
| State 4 | 0.275 | 0.321 |
| State 3u | −0.276 | 0.340 |
| RCR | −0.584 | **0.022** |
| RCRu | −0.480 | 0.070 |
| SRC | −0.172 | 0.540 |
| Mitochondrial mass biomarkers | | |
| Citrate synthase | 0.629 | **0.005** |
| mtDNA copy number | 0.030 | 0.915 |
| *mtDNA damage (%)* | | |
| Deletions in *CYTB* | −0.250 | 0.333 |
| Deletions in *ND4* | −0.265 | 0.304 |

Correlation parameters were obtained plotting individual values for CGG repeats and mitochondrial outcomes for 12 control and 5 premutation cell lines. Bolded $p$ values represent the presence of a statistically significant correlation between CGG repeats and a given mitochondrial outcome

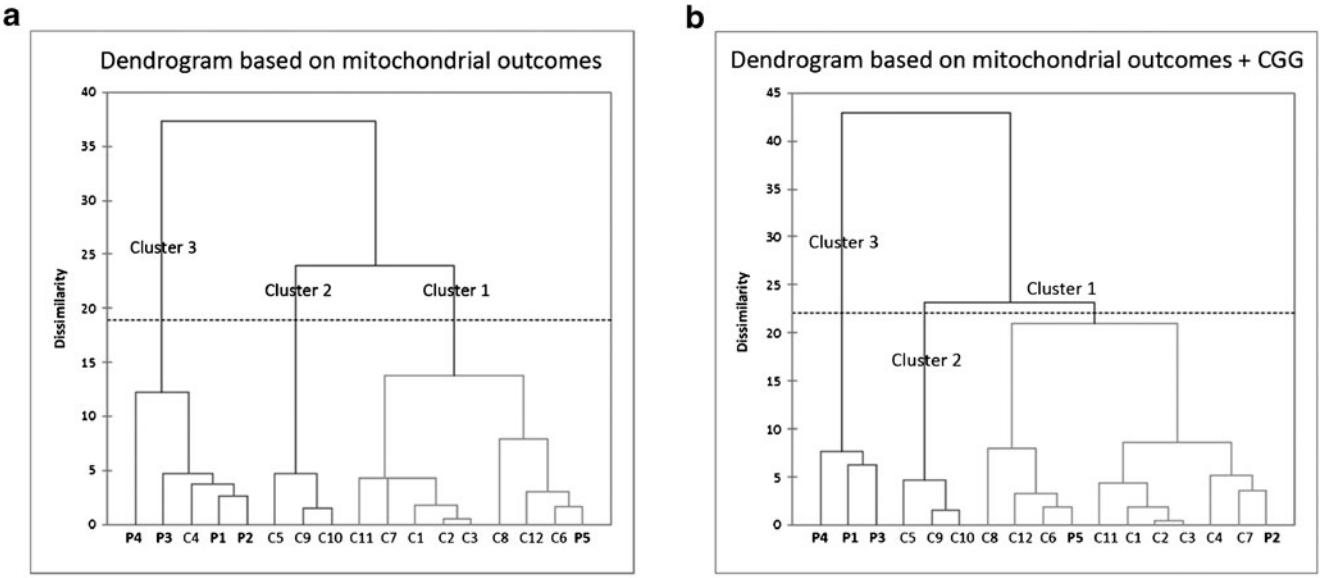


c

| Diagnostic test evaluation | | |
|---|---|---|
| **Parameter** | **Mitochondrial outcomes** | **Mitochondrial outcomes + CGG** |
| **Sensitivity** | 80% | 60% |
| **Specificity** | 92% | 100% |

**Fig. 4** Agglomerative clustering analysis of mitochondrial outcomes. An agglomerative hierarchical clustering (AHC) was performed utilizing all data collected in this study. The dissimilarity was based on the Euclidean distance, and Ward's was used as the agglomeration method (center and reduction, truncation automatic). The AHC analysis classified the donors into three clusters, which slightly differed whether the analysis was performed based on mitochondrial outcomes alone (**a**) or mitochondrial outcomes and CGG length (**b**). The comparison between the two agglomerative clustering analyses is shown in **c**. Parameters of the diagnostic test (calculated by the software MedCalc, version 16.2.1) are described as follows: *Sensitivity* = probability that a test result will be positive when the disease is present (true positive rate); *Specificity* = probability that a test result will be negative when the disease is not present (true negative rate). Both sensitivity and specificity are expressed as percentages

segments encoding for *CYTB* and *ND4* were observed between controls and premutation carriers (Fig. 1c and Supplementary Table 1). However, two of the five premutation samples (both included in cluster 3) presented lower mtDNA copy number (61 and 57 % of controls, respectively) whereas the remaining three premutation carriers had mtDNA copy number per cell >95 % CI (Supplementary Table 1). The low levels of mtDNA copy number, although significant, did not fulfill the criteria for mtDNA depletion syndrome (≤30 %) [33–35]. While low mtDNA levels have been reported during long-term use of antiretroviral agents, viral hepatitis, or iron storage diseases [36, 37], it has also been observed in premature ageing or failure in antagonizing long-term oxidative stress, especially in diabetes, heart failure, and cancer [38]. The fact that one of these samples (premutation no. 2) presented lower mtDNA copy number with increased deletions is indicative of defective mtDNA replication and/or maintenance with increased oxidative stress not compensated by antioxidant or repair defenses. While the mtDNA copy number is usually proportional to mitochondrial mass, changes in this number have been associated with increased oxidative stress and/or defects in transcription as well as with aberrant behavioral outcomes [39, 40]. Indeed, signs of increased mitochondrial oxidative stress were evident in the three other cell lines included in cluster 3 (premutation no. 1, no. 3, and no. 4) which showed mtDNA copy number per cell >95 % CI with increased deletions in at least one of the mtDNA segments tested; Supplementary Table 1).

## Concluding Remarks

A role for mitochondrial dysfunction has emerged as a common mechanism underlying many neurological disorders [8, 12, 41–43] including ASD [15, 18, 44] with specific detrimental outcomes, such as lower ATP production, increases in mitochondrial ROS, and/or metabolite inhibition of critical steps within mitochondrial pathways [45]. In this study, we tested for bioenergetics in fibroblasts from carriers of the premutation before a significant clinical involvement was observed. The most significant changes were increased citrate synthase activity, a generalized lower OXPHOS deficit and a

**Table 3** Comparison of mitochondrial outcomes in fibroblasts from younger and older adults with and without FXTAS

| Age (years) | Mitochondrial outcomes | | | | | Reference |
|---|---|---|---|---|---|---|
| | Complex I | Complex II | Complex IV | Complex V | Citrate synthase | |
| 28 ± 2 (asymptomatic) | 23 %* | N.D. | 51 %* | 64 % | 164 %* | This study |
| 71 ± 2 (asymptomatic) | 100 % | 142 % | 34 %* | 71 % | 74 % | [8] |
| 68 ± 3 (FXTAS-affected) | 75 % | 68 % | 56 %* | 38 %* | 100 % | [8] |

Activities are expressed as nmol × (min × mg protein)$^{-1}$, normalized by citrate synthase and expressed as percent of control values (age- and sex-matched), except citrate synthase

*N.D.* not determined

*$p < 0.05$ vs. age- and sex-matched controls

disrupted mitochondrial network, mitochondria morphology, and distribution. Although mitochondrial dysfunction has been observed in fibroblasts from older premutation patients [8, 12] and the severity of the dysfunction correlated with the occurrence of clinical symptoms [8, 12], this is the first report of a well-characterized mitochondrial impairment in relatively young carriers. In this regard, the presence of a strong correlation between some of the mitochondrial outcomes tested (ATP-linked oxygen uptake, coupling, citrate synthase activity, and the organization of the mitochondrial network) and the CGG repeat expansion in the fibroblasts obtained from younger premutation individuals without overt clinical symptoms is consistent with the correlation between severity of FXTAS symptoms in older individuals and increasing CGG repeat size [31]. Comparing the results obtained with younger carriers (this study) to those obtained previously with older premutation carriers with and without FXTAS (Table 3), the deficits in Complex IV were shared by both age groups, although at a different degree (51 % in younger adults, 34 and 56 % for asymptomatic and symptomatic >60-year-old carriers). Similarly to younger carriers, a clear deficit of Complex V was observed in older carriers with FXTAS only (Table 3), but in the latter case the deficit was more pronounced (by 2-fold). A more generalized OXPHOS deficit was observed in younger carriers with higher citrate synthase activity, whereas in older ones more specific Complex IV (asymptomatic and FXTAS-affected) and Complex V (only FXTAS-affected) deficits were observed [8].

The observed increases in citrate synthase activity could reflect an increase in the matrix content of mitochondria, which, along with the generalized decreases in electron transfer activity across Complexes, support the concept that the composition of mitochondrial compartments is altered in the premutation. If we were to consider activities of Complexes as references to evaluate the relative amount of the mitochondrial inner membrane and citrate synthase as a reference for matrix content, then these bioenergetic changes occurring in the premutation seem to result from an altered ratio among respiratory chain components and Krebs' cycle enzymes. This metabolic switch which includes a lower capacity to metabolize FAD-linked (succinate oxidase) than NAD-linked reducing equivalents (NADH oxidase, i.e., fatty acids over carbohydrates), and the higher citrate synthase activity, may indicate a more pro-inflammatory activity supported by the following: (i) Complex I is linked with an activation of the innate immune response state [46, 47], and (ii) the higher citrate synthase activity, which coupled to the citrate transporter, favors the synthesis of cytokine-induced inflammatory signals and prostaglandins [48, 49].

This "pro-inflammatory state" may contribute to the accumulation of mitochondrial and cellular damage. In this regard, mitochondrial dysfunction fuels a detrimental sequence of damage to critical biological targets through the generation of ROS. Increased ROS levels, inferred from the higher State 4-linked oxygen uptake observed in carriers' cells, may also damage mtDNA (as observed in increased mtDNA deletions in at least one of the genes tested in four of five carriers) which could sustain this feed-forward spiral of damage either by suppressing the expression of mtDNA-encoded genes for OXPHOS or by damaging the original mtDNA template [50]. As such, accumulation of mitochondrial damage may contribute to the emotional/developmental problems observed in younger carriers of the premutation and, more so, in the presence of FXTAS later in life.

Finally, mitochondrial dysfunction seems to be an incipient pathological process occurring in perhaps all triplet nucleotide repeat disorders [8, 9, 12], underlying the behavioral problems evident in some of these young carriers [5]. Taken together, mitochondrial dysfunction is already evident in fibroblasts from younger, presymptomatic premutation carriers, indicating that these deficits precede the onset and/or development of FXTAS and highlight the importance of mitochondrial outcomes as potential biomarker of prognosis.

**Acknowledgments** We wish to thank the subjects that provided the samples making this study possible, Dr. Paul Hagerman and Ms.

Glenda Espinal (Department of Biological Chemistry and Molecular Medicine, School of Medicine, University of California Davis) for providing the fibroblasts used in this study, and Dr. Flora Tassone (Department of Biochemistry and Molecular Medicine, School of Medicine, University of California, Davis) for assessing CGG repeat expansions in blood.

**Compliance with Ethical Standards**

**Funding** This study was funded by National Institutes for Health (ES12691, ES020392, HD036071, and HD040661) and Simons Foundation (no. 271406). Support was also obtained from the MIND Institute Intellectual and Developmental Disabilities Research Center (U54 HD079125).

**Conflict of Interest** R.H. has received funding from Novartis, Roche/Genentech, Alcobra, and Neuren for treatment trials in fragile X syndrome, autism, and Down syndrome. She has also consulted with Novartis, Zynerba, and Roche/Genentech regarding treatment for fragile X syndrome. The other authors have no financial disclosures relevant to this article.

## References

1. Suhl JA, Muddashetty RS, Anderson BR, Ifrim MF, Visootsak J, Bassell GJ, et al. A 3′ untranslated region variant in FMR1 eliminates neuronal activity-dependent translation of FMRP by disrupting binding of the RNA-binding protein HuR. Proc Natl Acad Sci U S A. 2015;112:E6553–61. doi:10.1073/pnas.1514260112.
2. Todd PK, Oh SY, Krans A, He F, Sellier C, Frazer M, et al. CGG repeat-associated translation mediates neurodegeneration in fragile X tremor ataxia syndrome. Neuron. 2013;78:440–55. doi:10.1016/j.neuron.2013.03.026.
3. Jin P, Warren ST. Understanding the molecular basis of fragile X syndrome. Hum Mol Genet. 2000;9:901–8.
4. Hatton DD, Sideris J, Skinner M, Mankowski J, Bailey Jr DB, Roberts J, et al. Autistic behavior in children with fragile X syndrome: prevalence, stability, and the impact of FMRP. Am J Med Genet A. 2006;140A:1804–13. doi:10.1002/ajmg.a.31286.
5. Hagerman R, Hagerman P. Advances in clinical and molecular understanding of the FMR1 premutation and fragile X-associated tremor/ataxia syndrome. Lancet Neurol. 2013;12:786–98. doi:10.1016/S1474-4422(13)70125-X.
6. Kogan CS, Turk J, Hagerman RJ, Cornish KM. Impact of the Fragile X mental retardation 1 (FMR1) gene premutation on neuropsychiatric functioning in adult males without fragile X-associated Tremor/Ataxia syndrome: a controlled study. Am J Med Genet B Neuropsychiatr Genet. 2008;147B:859–72. doi:10.1002/ajmg.b.30685.
7. Tassone F, Iwahashi C, Hagerman PJ. FMR1 RNA within the intranuclear inclusions of fragile X-associated tremor/ataxia syndrome (FXTAS). RNA Biol. 2004;1:103–5.
8. Napoli E, Ross-Inta C, Wong S, Omanska-Klusek A, Barrow C, Iwahashi C, et al. Altered zinc transport disrupts mitochondrial protein processing/import in fragile X-associated tremor/ataxia syndrome. Hum Mol Genet. 2011;20:3079–92. doi:10.1093/hmg/ddr211.
9. Napoli E, Wong S, Hung C, Ross-Inta C, Bomdica P, Giulivi C. Defective mitochondrial disulfide relay system, altered mitochondrial morphology and function in Huntington's disease. Hum Mol Genet. 2013;22:989–1004. doi:10.1093/hmg/dds503.
10. Banez-Coronel M, Porta S, Kagerbauer B, Mateu-Huertas E, Pantano L, Ferrer I, et al. A pathogenic mechanism in Huntington's disease involves small CAG-repeated RNAs with neurotoxic activity. PLoS Genet. 2012;8:e1002481. doi:10.1371/journal.pgen.1002481.
11. Pearson CE. Repeat associated non-ATG translation initiation: one DNA, two transcripts, seven reading frames, potentially nine toxic entities! PLoS Genet. 2011;7:e1002018. doi:10.1371/journal.pgen.1002018.
12. Ross-Inta C, Omanska-Klusek A, Wong S, Barrow C, Garcia-Arocena D, Iwahashi C, et al. Evidence of mitochondrial dysfunction in fragile X-associated tremor/ataxia syndrome. Biochem J. 2010;429:545–52. doi:10.1042/BJ20091960.
13. Liu J, Koscielska KA, Cao Z, Hulsizer S, Grace N, Mitchell G, et al. Signaling defects in iPSC-derived fragile X premutation neurons. Hum Mol Genet. 2012;21:3795–805. doi:10.1093/hmg/dds207.
14. Napoli E, Ross-Inta C, Song G, Wong S, Hagerman R, Gane L, et al. Premutation in the fragile X mental retardation 1 (FMR1) gene affects maternal Zn-milk and perinatal brain bioenergetics and scaffolding. Front Neurosci. 2016. doi:10.3389/fnins.2016.00159.
15. Giulivi C, Zhang YF, Omanska-Klusek A, Ross-Inta C, Wong S, Hertz-Picciotto I, et al. Mitochondrial dysfunction in autism. JAMA. 2010;304:2389–96. doi:10.1001/jama.2010.1706.
16. Napoli E, Hung C, Wong S, Giulivi C. Toxicity of the flame-retardant BDE-49 on brain mitochondria and neuronal progenitor striatal cells enhanced by a PTEN-deficient background. Toxicol Sci. 2013;132:196–210. doi:10.1093/toxsci/kfs339.
17. Napoli E, Ross-Inta C, Wong S, Hung C, Fujisawa Y, Sakaguchi D, et al. Mitochondrial dysfunction in Pten haplo-insufficient mice with social deficits and repetitive behavior: interplay between Pten and p53. PLoS One. 2012;7:e42504. doi:10.1371/journal.pone.0042504.
18. Napoli E, Wong S, Giulivi C. Evidence of reactive oxygen species-mediated damage to mitochondrial DNA in children with typical autism. Mol Autism. 2013;4:2. doi:10.1186/2040-2392-4-2.
19. Vowinckel J, Hartl J, Butler R, Ralser M. MitoLoc: a method for the simultaneous quantification of mitochondrial network morphology and membrane potential in single cells. Mitochondrion. 2015;24:77–86. doi:10.1016/j.mito.2015.07.001.
20. Hackenbrock CR. Ultrastructural bases for metabolically linked mechanical activity in mitochondria. II. Electron transport-linked ultrastructural transformations in mitochondria. J Cell Biol. 1968;37:345–69.
21. Buffa P, Pasquali-Ronchetti I. Biochemical lesions of respiratory enzymes and configurational changes of mitochondria in vivo. II. Early ultrastructural modifications correlated to the biochemical lesion induced by fluoroacetate. Cell Tissue Res. 1977;183:1–23.
22. Cooper JM, Petty RK, Hayes DJ, Challiss RA, Brosnan MJ, Shoubridge EA, et al. An animal model of mitochondrial myopathy: a biochemical and physiological investigation of rats treated in vivo with the NADH-CoQ reductase inhibitor, diphenyleneiodonium. J Neurol Sci. 1988;83:335–47.
23. Chance B, Hollunger G. Inhibition of electron and energy transfer in mitochondria. IV. Inhibition of energy-linked diphosphopyridine nucleotide reduction by uncoupling agents. J Biol Chem. 1963;238:445–8.
24. Chance B, Williams GR, Hollunger G. Inhibition of electron and energy transfer in mitochondria. III. Spectroscopic and respiratory effects of uncoupling agents. J Biol Chem. 1963;238:439–44.
25. Okuda M, Lee HC, Kumar C, Chance B. Comparison of the effect of a mitochondrial uncoupler, 2,4-dinitrophenol and adrenaline on oxygen radical production in the isolated perfused rat liver. Acta Physiol Scand. 1992;145:159–68. doi:10.1111/j.1748-1716.1992.tb09351.x.

26. Jastroch M, Divakaruni AS, Mookerjee S, Treberg JR, Brand MD. Mitochondrial proton and electron leaks. Essays Biochem. 2010;47:53–67. doi:10.1042/bse0470053.
27. Fiskum G, Murphy AN, Beal MF. Mitochondria in neurodegeneration: acute ischemia and chronic neurodegenerative diseases. J Cereb Blood Flow Metab. 1999;19:351–69. doi:10.1097/00004647-199904000-00001.
28. Nicholls DG. Mitochondrial function and dysfunction in the cell: its relevance to aging and aging-related disease. Int J Biochem Cell Biol. 2002;34:1372–81.
29. Chan DC. Mitochondrial fusion and fission in mammals. Annu Rev Cell Dev Biol. 2006;22:79–99. doi:10.1146/annurev.cellbio.22.010305.104638.
30. Perry SW, Norman JP, Barbieri J, Brown EB, Gelbard HA. Mitochondrial membrane potential probes and the proton gradient: a practical usage guide. Biotechniques. 2011;50:98–115. doi:10.2144/000113610.
31. Leehey MA. Fragile X-associated tremor/ataxia syndrome: clinical phenotype, diagnosis, and treatment. J Investig Med. 2009;57:830–6. doi:10.231/JIM.0b013e3181af59c4.
32. Bernier FP, Boneh A, Dennett X, Chow CW, Cleary MA, Thorburn DR. Diagnostic criteria for respiratory chain disorders in adults and children. Neurology. 2002;59:1406–11.
33. Miro O, Lopez S, Pedrol E, Rodriguez-Santiago B, Martinez E, Soler A, et al. Mitochondrial DNA depletion and respiratory chain enzyme deficiencies are present in peripheral blood mononuclear cells of HIV-infected patients with HAART-related lipodystrophy. Antivir Ther. 2003;8:333–8.
34. Mancuso M, Filosto M, Bonilla E, Hirano M, Shanske S, Vu TH, et al. Mitochondrial myopathy of childhood associated with mitochondrial DNA depletion and a homozygous mutation (T77M) in the TK2 gene. Arch Neurol. 2003;60:1007–9. doi:10.1001/archneur.60.7.1007.
35. Yano S, Li L, Le TP, Moseley K, Guedalia A, Lee J, et al. Infantile mitochondrial DNA depletion syndrome associated with methylmalonic aciduria and 3-methylcrotonyl-CoA and propionyl-CoA carboxylase deficiencies in two unrelated patients: a new phenotype of mtDNA depletion syndrome. J Inherit Metab Dis. 2003;26:481–8.
36. Miro O, Lopez S, Cardellach F, Casademont J. Mitochondrial studies in HAART-related lipodystrophy: from experimental hypothesis to clinical findings. Antivir Ther. 2005;10 Suppl 2: M73–81.
37. Muller-Hocker J, Muntau A, Schafer S, Jaksch M, Staudt F, Pongratz D, et al. Depletion of mitochondrial DNA in the liver of an infant with neonatal giant cell hepatitis. Hum Pathol. 2002;33:247–53.
38. Kang D, Hamasaki N. Alterations of mitochondrial DNA in common diseases and disease states: aging, neurodegeneration, heart failure, diabetes, and cancer. Curr Med Chem. 2005;12:429–41.
39. Liu CS, Tsai CS, Kuo CL, Chen HW, Lii CK, Ma YS, et al. Oxidative stress-related alteration of the copy number of mitochondrial DNA in human leukocytes. Free Radic Res. 2003;37:1307–17.
40. Ylikallio E, Tyynismaa H, Tsutsui H, Ide T, Suomalainen A. High mitochondrial DNA copy number has detrimental effects in mice. Hum Mol Genet. 2010;19:2695–705. doi:10.1093/hmg/ddq163.
41. Chu CT. A pivotal role for PINK1 and autophagy in mitochondrial quality control: implications for Parkinson disease. Hum Mol Genet. 2010;19:R28–37. doi:10.1093/hmg/ddq143.
42. St-Pierre J, Drori S, Uldry M, Silvaggi JM, Rhee J, Jager S, et al. Suppression of reactive oxygen species and neurodegeneration by the PGC-1 transcriptional coactivators. Cell. 2006;127:397–408. doi:10.1016/j.cell.2006.09.024.
43. Pathak D, Berthet A, Nakamura K. Energy failure: does it contribute to neurodegeneration? Ann Neurol. 2013;74:506–16. doi:10.1002/ana.24014.
44. Napoli E, Wong S, Hertz-Picciotto I, Giulivi C. Deficits in bioenergetics and impaired immune response in granulocytes from children with autism. Pediatrics. 2014;133:e1405–10. doi:10.1542/peds.2013-1545.
45. Johri A, Beal MF. Mitochondrial dysfunction in neurodegenerative diseases. J Pharmacol Exp Ther. 2012;342:619–30. doi:10.1124/jpet.112.192138.
46. Cloonan SM, Choi AM. Mitochondria: commanders of innate immunity and disease? Curr Opin Immunol. 2012;24:32–40. doi:10.1016/j.coi.2011.11.001.
47. Chen Y, Lu H, Liu Q, Huang G, Lim CP, Zhang L, et al. Function of GRIM-19, a mitochondrial respiratory chain complex I protein, in innate immunity. J Biol Chem. 2012;287:27227–35. doi:10.1074/jbc.M112.340315.
48. Napoli E, Tassone F, Wong S, Angkustsiri K, Simon TJ, Song G, et al. Mitochondrial citrate transporter-dependent metabolic signature in the 22q11.2 deletion syndrome. J Biol Chem. 2015;290:23240–53. doi:10.1074/jbc.M115.672360.
49. Infantino V, Iacobazzi V, Menga A, Avantaggiati ML, Palmieri F. A key role of the mitochondrial citrate carrier (SLC25A1) in TNFalpha- and IFNgamma-triggered inflammation. Biochim Biophys Acta. 1839;2014:1217–25. doi:10.1016/j.bbagrm.2014.07.013.
50. Yakes FM, Van Houten B. Mitochondrial DNA damage is more extensive and persists longer than nuclear DNA damage in human cells following oxidative stress. Proc Natl Acad Sci U S A. 1997;94:514–9.